Liquid-Phase Structure of Dialkylimidazolium Ionic Liquids from Computer Simulations

Jones de Andrade, Elvis S. Böes, and Hubert Stassen*

Grupo de Química Teórica, Instituto de Química, Universidade Federal do Rio Grande do Sul, Av. Bento Gonçalves 9500, 91540-000, Porto Alegre - RS, Brazil

Received: February 18, 2008; Revised Manuscript Received: May 2, 2008

We present a detailed computational study of the structure of ionic liquids based on the imidazolium cation. Both imidazolium-ring stacking and hydrogen bonding behavior are investigated from radial and spatial orientational distribution functions, as well as orientational correlation functions. The alkyl chain size and anion effect on the liquid structure are provided and discussed. Our results support models for liquid organization comparable to those formulated on the basis of experimental observations.

1. Introduction

In the last decades, both public concerns and more rigorous legislation respecting environmental awareness and the protection of natural resources motivated the chemistry community to invest in the so-called green technologies.[1] As an example, one might cite research on alternatives to common organic solvents being substituted by supercritical fluids,[2] perfluorinated solvents,[3] and ionic liquids.[4]

The ionic liquids represent an interesting solvent class for many reasons. They are almost nonvolatile,[5] good solvents for a broad range of organic and inorganic materials, possess huge stability against strong reaction media, and are utilized in a large number of chemical syntheses.[6] Motivated by these interesting and intriguing properties, the number of experimental studies on ionic liquids has grown enormously in the last two decades.[7] However, only in recent years have computational and theoretical studies on such systems been described in the literature. We mention some isolated molecule and ion pair studies using quantum mechanical (QM) approaches[8–21] and, more recently, studies focusing on liquid-state characteristics by molecular dynamics (MD) or Monte Carlo simulations[22] and coarse-graining MD.[23–25] Also, studies concerning liquid-state interactions from a QM point of view[26–30] and others involving polarization effects in ionic liquids[31,32] have been described.

Recently, we published a complete flexible all-atom force field for imidazolium-based salts[33,34] within the AMBER force field and parameter development methodologies.[35] In ref 36, we have demonstrated that the developed parameters for four room-temperature molten salts composed of 1-ethyl-3-methylimidazolium (C_2C_1im) and 1-*n*-butyl-3-methylimidazolium (C_4C_1im) cations and tetrachloroaluminate ($AlCl_4^-$) and tetrafluoroborate (BF_4^-) anions reproduce many physical−chemical experimental properties of the ionic liquids (ILs) very well. We will refer to these salts in the remainder of the article as C_2C_1im$AlCl_4$, C_2C_1imBF_4, C_4C_1im$AlCl_4$, and C_4C_1imBF_4.

Also, in these publications, some initial insight into the ionic liquids structural features has been undertaken. Here, we detail this specific subject, making use of the previously developed force field. Many of the important ionic liquids' physical properties are supposed to be directly related to their liquid-phase structure. Although experimental access to structural details in condensed phases is rather difficult, some basic models of the IL structure are provided in the literature,[37–39] revealing cation−cation ring stacking,[40,41] hydrogen bonding between cations and anions,[42–45] and the parallel orientation of alkyl chains from different cations.[24,46] In the present study, we provide a more detailed study of the IL structure. For this purpose, we make use of site−site radial distribution functions (RDFs), several well-chosen spatial distribution functions (SDFs), 2D and 3D spatial density functions (2D and 3D SDFs), and orientational correlation functions (OCFs). From these properties, the microscopic liquid-phase structural characteristics, such as imidazolium-ring stacking and hydrogen bonding between cations and anions, are revealed. Moreover, the dependence of the liquid-phase structure on microscopical characteristics of the ions is discussed. Here, we emphasize the influence of the size of the alkyl chain by studying ILs based on the $C_2C_1im^+$ and the $C_4C_1im^+$ cations, as well as the choice of the anion employing $AlCl_4^-$ and BF_4^- anions. Finally, some qualitative relationships between the liquid-phase structure and macroscopical properties are provided.

TABLE 1: Experimental ϱ_{exp}[43,56,57,58] and Simulated ϱ_{sim} Densities (in g/cm ^{3}), Position of the First Maxima in the Cation−Cation RDFs (in Angstroms), and Their Normalized Integrals (in Parentheses) for the Simulated ILs

IL	*T*/K	ϱ_{exp}	ϱ_{sim}	prepeak	peak
C_2C_1im$AlCl_4$	298	1.302	1.363		9.6 (10.4)
C_4C_1im$AlCl_4$	298	1.238	1.238		12.5 (19.1)
C_2C_1imBF_4	295	1.24	1.253	5.1 (0.9)	10.7 (19.3)
C_4C_1imBF_4	303	1.17	1.172	4.8 (0.4)	11.0 (16.9)

2. Methods

We have carried out MD simulations on the ILs described above composed by 128 pairs of cations and anions. The simulations were performed with the MDynaMix program[47] using self-written codes for further analysis of the trajectories. The $C_2C_1im^+$ and $C_4C_1im^+$ cations, as well as the $AlCl_4^-$ and BF_4^- anions, were modeled by our previously published force field.[33,34] All the results presented here were obtained from simulations within the *NpT* ensemble (Nosé-Hoover thermostat, coupling constant of 30 fs; Nosé-Hoover barostat, coupling constant of 400 fs [48]) at a pressure of 1 atm and temperatures close to 300 K. (See Table 1 for the exact temperatures.) Starting from a cubic simulation box containing randomly arranged ion pairs under periodic boundary conditions and minimum image

* Corresponding author. E-mail: gullit@iq.ufrgs.br.

10.1021/jp801445j CCC: $40.75
Published on Web 07/02/2008

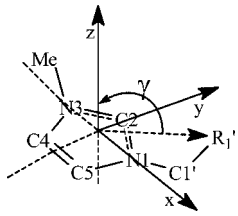

Figure 1. Local coordinate system for the imidazolium rings.

convention, a double time-step algorithm[49] was used to solve the equations of motions with the large time step fixed at 2 fs and the shorter at 0.2 fs. The equilibration period in each MD run was at least 200 ps, and the production runs were extended to more than 100 ps. Configurations were saved for further analysis in intervals of five time steps (10 fs). In all the simulations, the cutoff radius was kept to 17 Å. This distance also represents the real-space cutoff radius for the Ewald summation[50] employed in the treatment of electrostatic forces. The equilibration phase was monitored by plotting the total, kinetic, intermolecular, and intramolecular potential energies as a function of the simulated time.

The structure of the ILs was studied utilizing three different functions: site−site radial distribution functions, spatial distribution functions (the common SDFs and the 3D SDFs), and orientational correlation functions.[51] Their mathematical definitions as well as the atoms, molecular sites, local coordinate systems, and vectors employed in the calculations are presented in the following.

The RDFs involve different pairs of sites, such as specific atoms of cations and anions, or origins of local coordinate systems for the cations. This origin was defined here to be the geometric center between the two imidazolium-ring nitrogen atoms. In any case, for a given number density $\varrho = N/V$ of N molecules within a volume V, the RDF describing the correlation between two sites a and b possesses the functional form

$$g_{ab}(r) = \frac{1}{N\varrho}\left\langle \sum_{i=1}^{N_a}\sum_{j\neq i}^{N_b} \delta(r - r_{ij}) \right\rangle \quad (1)$$

where N_a and N_b refer to the number of a and b sites separated by r_{ij}.

Additional correlations of the distances r_{ij} with some characteristic angles θ_{ij} define the SDFs and OCFs,

$$g_{ab}(r,\theta) = \frac{1}{N\varrho}\left\langle \sum_{i=1}^{N_a}\sum_{j\neq i}^{N_b} \delta(r - r_{ij})\,\delta(\theta - \theta_{ij}) \right\rangle \quad (2)$$

The particular definition of the angle θ distinguishes SDFs from OCFs as described below.

The 3D SDF is intuitively similar and is defined by

$$g_{a,b}(x,y,z) = \frac{1}{N\varrho}\left\langle \sum_{i=1}^{N_a}\sum_{j\neq i}^{N_b} \delta(x - x_{ij})\,\delta(y - y_{ij})\,\delta(z - z_{ij}) \right\rangle \quad (3)$$

with x_{ij}, y_{ij}, and z_{ij} representing the Cartesian components of the distance vector r_{ij} between sites i and j. Although not giving a proper and quantitative view of the structures, the 3D SDFs present a qualitative view of the coordinating regions for the b sites around the a sites.

The axes of the cation's local coordinate system were defined as follows: the origin of the system is placed at the geometric center between the two nitrogen atoms of the imidazolium ring. As illustrated in Figure 1, the unit vector pointing to the N1 nitrogen defines the x axis and the unit vector to the C2 carbon

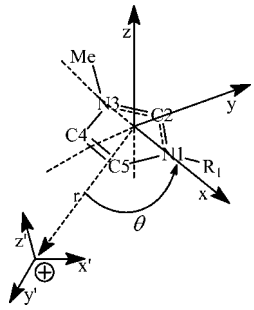

Figure 2. Schematic definition of the SDFs for pairs of cations.

defines the y axis. These two unit vectors are almost perfectly perpendicular during the simulations,[33,34] with minor deviations from perpendicularity caused by thermal distortions of the ring skeleton. Orthogonal to these two unit vectors, the z axis is defined as indicated in Figure 1. Because of the asymmetric substitutions in the cation's molecular structure, this definition hides the alkyl chain effect on the structure in this coordinate axis. Thus, we used the angle γ as indicated in the left panel of Figure 1 to define the z axis as always pointing to that side of the ring where the alkyl chain's second carbon (C2′) is located (the R_1' in Figure 1). This approach is supported by both the equilibrium dihedral angle between the ring plane and the C2′ atom and the observed small fluctuations in this torsional angle confirmed by our MD simulations. The analysis of the torsional profiles indicates more perpendicular configurations for this dihedral.

At this point, we introduce nomenclature to be used in the remainder of the article. Henceforth, we will call the region surrounding the positive side of the y axis, which corresponds to the region around the H2 hydrogen, the "front". However, the negative side of the y axis, corresponding to the region around and in between the H4 and H5 hydrogens, is called the "back". Moreover, the regions around the positive and negative sides of the z vector will be considered "over" and "under", respectively. Finally, the region surrounding the cation's xy plane is labeled as the "equatorial region".

From these definitions, an OCF for the cations can be defined by angles θ between the coordinate axes of different cations. In this study, angles between the x, y, and z axes for pairs of molecules separated by a site−site distance r are considered in order to produce some insight into the proposed imidazolium-ring stacking of the ionic liquids. However, the SDFs do not involve angles θ between coordinate axes of a pair of molecules but between a molecule's coordinate axis and the distance vector r separating the pair. Figure 2 represents an illustration of these considerations for the particular case with θ defined as the angle between the cation's x axis and r. The 3D SDF simultaneously correlates the Cartesian components of the separation vector r. Thus, although not involving explicitely angular terms in its definition from eq 3, a space distribution of neighboring positions around a defined orientation of a central molecule can be obtained.

In a similar way, the cation−anion SDFs were defined. Here, the reference vector r is taken to be the vector between the origin of the cation and the atoms of the anions. As in Figure 2, the angle θ is defined between this reference vector and one of the cation coordinate axes. The 3D SDFs for the cation−anion distribution considers correlations of the Cartesians components of this reference vector. The anion−anion structural features are discussed in terms of RDFs. Because of the tetrahedral symmetries of the involved anions, a more detailed discussion of interanionic orientational arrangements is obsolete.

3. Results and Discussion

3.1. Cation−Cation Structure. In this section, we present details on the cation−cation structure in the ILs. This involves a discussion of the presumed stacking of the imidazolium rings that has been postulated on the basis of NMR studies.[52,53] Solid-phase scattering and diffraction studies corroborate this kind of structural organization on different length scales depending on the ionic liquid.[54,55]

Moreover, the nature of the anion influences this structural feature of the ILs. Often treated only as a partner in the discussion of structural features in ILs, our results here suggest that the choice of the anion strongly affects the IL structure, especially in sustaining or breaking the cation−cation stacking.

Most of the liquid-state simulations on ILs described in the literature so far (see refs[59–61] for exceptions) consider anions with spherical symmetry: Cl^-, Br^-, BF_4^-, $AlCl_4^-$, PF_6^-, and so forth. Thus, their differences, when excluding polarization effects as in this work, are restricted to geometric terms such as the radius, volume, and surface area. In this work, we focus on two anions, $AlCl_4^-$ and $BF4_4^-$. Both anions possess T_d symmetry. $AlCl_4^-$ is significantly larger than the BF_4^-; consequently, when comparing structural data for both, the size effect of the anions is revealed.

In Figure 3, we have depicted the cation−cation RDFs. At a glance, these RDFs exhibit very similar behavior at intermediate to long distances. However, on the short-range flank of the first maximum, we observe major differences. The $AlCl_4^-$ containing ILs produces short-range peak broadening, which appears as prepeaks in the ILs with the BF_4^- anion. The increased tendency to form more pronounced short-range configurations in BF_4^- containing ILs is probably a density effect (Table 1) that is expected for ILs containing smaller anions. In Figure 3, we also present the partial RDFs for the five closest neighbors. Normalized integrals for the RDFs are listed in Table 1. These properties indicate that the short-range prepeak appearing in the ILs with BF_4^- anions corresponds to a single nearest neighbor. The partial RDFs from Figure 3 confirm that the short distance shoulder in the first peak of the $AlCl_4^-$ containing ILs also contains a single cation. However, the principal differences between $AlCl_4^-$ and BF_4^- containing ILs originate at the most probable distance for finding the nearest neighbor that is dislocated by approximately 2 Å toward smaller distances in the BF_4^--based ILs. The partial RDFs for the next four neighbors build the RDF up to distances corresponding to the peak position of the first maximum. These findings suggest that the BF_4^--based ILs exhibit a more packed cation−cation structure with a distinguished nearest neighbor, which is differently from the structure of $AlCl_4^-$-based ILs.

In combining the SDFs and OCFs corresponding to the RDFs for the cation−cation pairs, we can obtain structural details for the first coordination shell. In Figures 4 and 5, contour plots of cation−cation SDFs for the four ILs are presented. In Figure 4, we have chosen the distribution around the z axis projected into the yz plane to filter the above and below regions of the cations. Figure 5 exhibits the distributions around the y axis. The SDF is projected into the xy plane (ring plane) in order to emphasize the front and behind regions of the cations. From the larger extent of warmer colors in these SDFs, it becomes evident that ILs based on BF_4^- anions possess a more tight organization than does $AlCl_4^-$ containing ILs. This becomes more noticeable in Figure 4, where the above (positive ordinate in Figure 4) and the below (negative ordinate in Figure 4) regions of the imidazolium ring exhibit stronger contributions. Moreover, the nearest and second nearest cations are more dislocated in the $AlCl_4^-$-based ILs. However, in the case of ILs containing

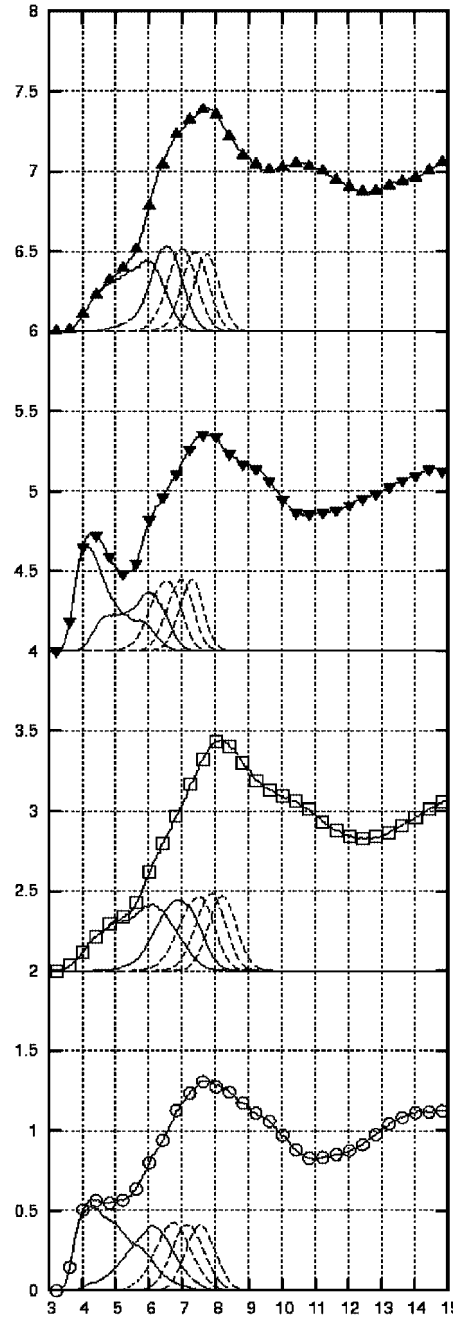

Figure 3. Cation−cation RDFs for the studied ILs from Table 1: ▲ (shifted by 6), $C_2C_1imAlCl_4$; ▼ (shifted by 4), $C_2C_1imBF_4$; □ (shifted by 2), $C_4C_1imAlCl_4$; and ○, $C_4C_1imBF_4$. For each IL, the partial RDFs for the first five neighbors (low-intensity functions from the left to right, in going from the first to the fifth nearest neighbor) are also presented.

BF_4^- anions, it is evident that the first and the second closest cations preferably stay above and below the imidazolium ring. This finding is in perfect agreement with the supposed stacking structure of cations in ILs. However, such a preference is not evident in the $AlCl_4^-$-based ILs: the first cation is preferably located below the imidazolium ring, whereas the second nearest cation is more delocalized. This indicates that cation−cation stacking in ILs strongly depends on the choice of the anion. Here, we observed that smaller anions produce a higher liquid density with an increased tendency toward cation−cation packing and stacking.

The cation−cation and cation−anion 3D SDFs for the $C_2C_1imBF_4$ and $C_2C_1imAlCl_4$ ILs confirm this aspect as

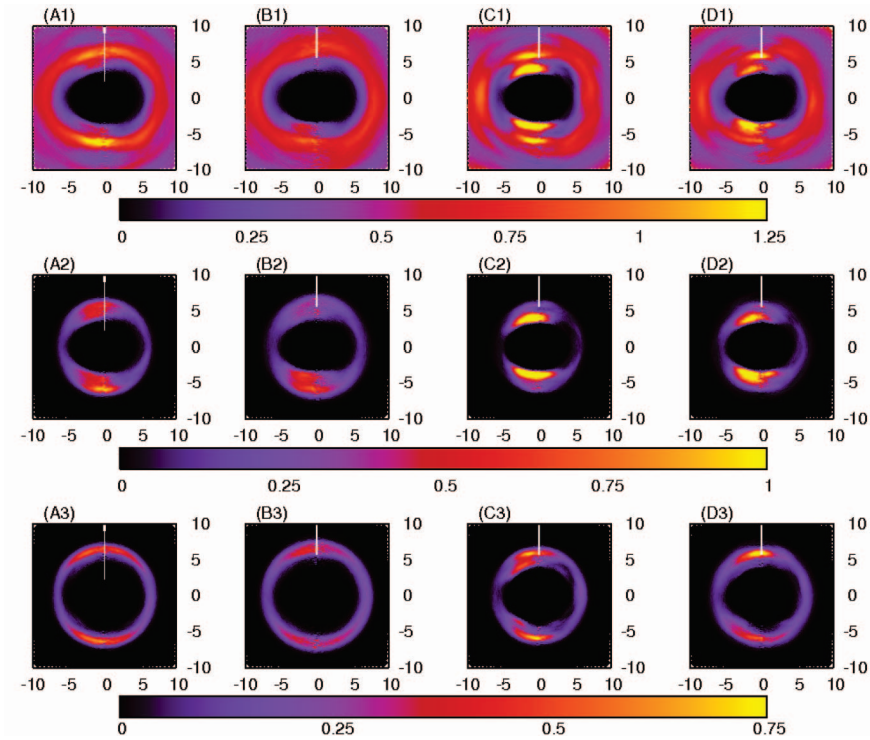

Figure 4. Cation−cation SDFs, measured around the *z* axis and projected into the *yz* plane: (A1) $C_2C_1imAlCl_4$, (B1) $C_4C_1imAlCl_4$, (C1) $C_2C_1imBF_4$, and (D1) $C_4C_1imBF_4$. Nearest neighbor for (A2) $C_2C_1imAlCl_4$, (B2) $C_4C_1imAlCl_4$, (C2) $C_2C_1imBF_4$, and (D2) $C_4C_1imBF_4$. Second nearest neighbor for (A3) $C_4C_1mAlCl_4$, (B3) $C_4C_1imAlCl_4$, (C3) $C_2C_1imBF_4$, and (D3) $C_4C_1imBF_4$.

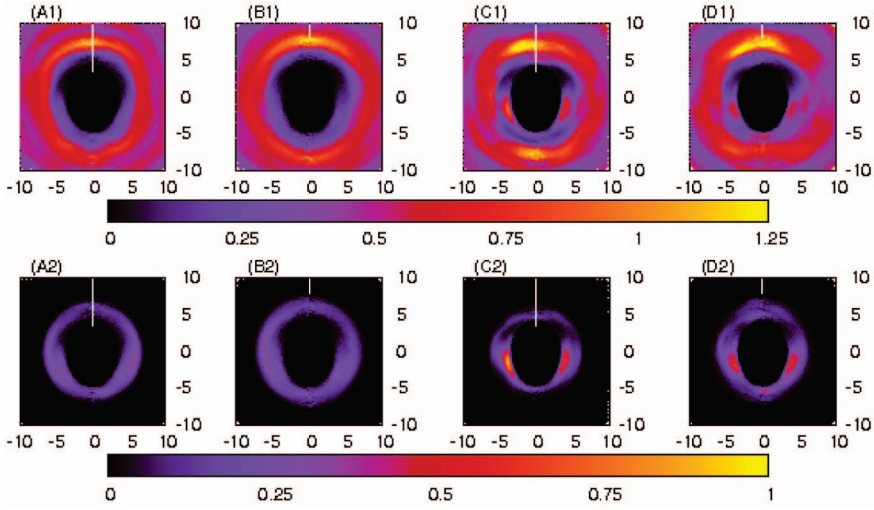

Figure 5. Cation−cation SDFs measured around the *y* axis and projected into the *xy* plane. (A1) $C_2C_1imAlCl_4$, (B1) $C_4C_1imAlCl_4$, (C1) $C_2C_1imBF_4$, and (D1) $C_4C_1imBF_4$. Nearest neighbor for (A2) $C_2C_1imAlCl_4$, (B2) $C_4C_1imAlCl_4$, (C2) $C_2C_1imBF_4$, and (D2) $C_4C_1imBF_4$.

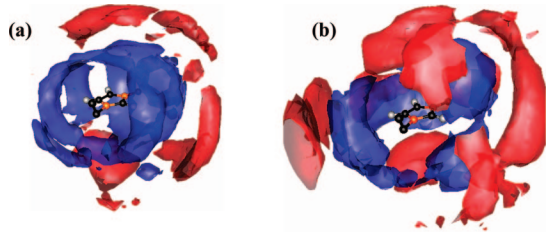

Figure 6. Cation−cation pairs (in red, isosurface 1.7) and cation−anion pairs (in blue, isosurface 2.0), and full 3D SDFs around the $C_2C_1im^+$ cation: (a) $C_2C_1imAlCl_4$ and (b) $C_2C_1imBF_4$.

illustrated in Figure 6. We found that, to a certain degree, the $AlCl_4^-$ anions disturb the placement of cations above and below the ring. In $C_2C_1imBF_4$, the above and below regions possess a strong preference for the location of cations, with the anions placed in the equatorial region.

Figures 4 and 5 also demonstrate the alkyl chain size effect on cation−cation coordination. Figure 4 demonstrates that an increase in the alkyl chain from ethyl to *n*-butyl ($C_2C_1im^+$ to $C_4C_1im^+$) leads to a decrease in the cation population above and below the imidazolium ring as a result of the steric effect of the longer alkyl chain. Figure 5 indicates that the behind region is slightly preferred when compared to the front region, probably as a result of the same steric effects. Moreover, Figure 4 suggests that the alkyl chain size favors the nearest neighbor below the ring and the second nearest cation above the imidazolium ring.

OCFs for cation−cation pairs containing orientational correlations between the *z* axes of the local coordinate systems are

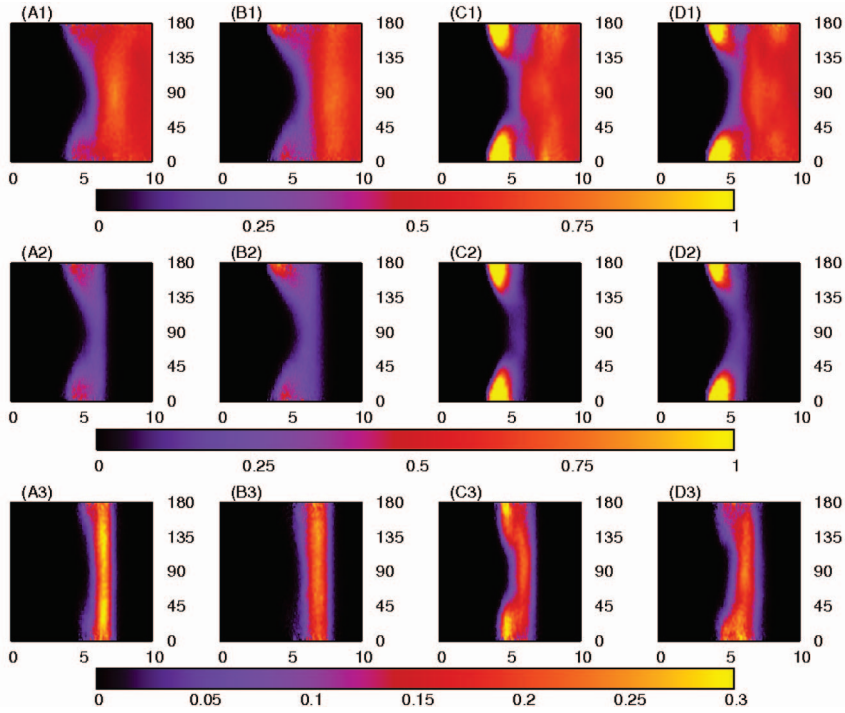

Figure 7. Cations OCFs containing correlations between molecular z axes: (A1) $C_2C_1imAlCl_4$, (B1) $C_4C_1imAlCl_4$, (C1) $C_2C_1imBF_4$, and (D1) $C_4C_1imBF_4$. Nearest neighbor for (A2) $C_2C_1imAlCl_4$, (B2) $C_4C_1imAlCl_4$, (C2) $C_2C_1imBF_4$, and (D2) $C_4C_1imBF_4$. Second nearest neighbor for (A3) $C_2C_1imAlCl_4$, (B3) $C_4C_1imAlCl_4$, (C3) $C_2C_1imBF_4$, and (D3) $C_4C_1imBF_4$.

illustrated in Figure 7. Also included are the OCFs for the nearest and the second nearest neighbors. At a glance, this Figure corroborate that the cation pairs are more tightly coordinated in the ILs containing BF_4^- anions, as has been concluded from the SDFs. Moreover, the nearest neighbors for all of the ILs, as well as the second nearest neighbors for the BF_4^--based ILs, exhibit preferred angles of 0 and 180° between the z axes, indicating parallel and antiparallel configurations of the ring planes. These observations are in perfect agreement with the supposed cation−cation stacking concluded from the SDFs. In addition, the preference for parallel and antiparallel relative orientation of the imidazolium rings is affected by the anion being more pronounced for the BF_4^--containing ILs.

In Figure S1 of the accompanying Supporting Information, we present OCFs with orientational correlation between molecular x axes for the cation pairs. This illustration produces a more detailed picture for both above and below coordination. The $AlCl_4^-$-based ILs produce only small orientational correlations between the x and y axes, whereas BF_4^- containing ILs exhibit some tendencies. Figure S1 shows that the first and second nearest cations in $C_2C_1imBF_4$ possess a preference for a 0° angle between the x axes. These arrangements indicate a certain degree of piling up of the ethyl substituents. In the case of $C_4C_1imBF_4$, additional smaller correlations at 180° are obtained for the nearest neighbor. However, the second nearest neighbor in this IL presents a preference for the 180° orientation, indicating that methyl groups of one cation orient toward the n-butyl groups of other cations.

However, OCFs for cation pairs sampled by correlating molecular orientations between the y axes, as shown in Figure S2 of the accompanying Supporting Information, present almost isotropic distributions, especially for the nearest neighbor. A small preference appears for the second nearest cation in BF_4^--based ILs at an angle of 180°. These correlations point to a starred configuration between the neighbors, with the H2 atom from one cation close to the H4 and H5 atoms of the other. However, this correlation is very weak and is easily turned into an almost isotropic distribution.

In summary, the cation−cation structural features indicate that the simulations reproduce the experimentally predicted stacking of imidazolium rings in the ILs. It is demonstrated that this stacking is related to the choice of the anion by density effects. Finally, the alkyl chain size affects the structural parameters of the ILs only slightly, at least for the ethyl and n-butyl substituents discussed here.

3.2. Cation−Anion Structure. The coordination of the imidazolium-ring hydrogen atoms (H2, H4, and H5) and the external atoms of the anions (Cl for $AlCl_4^-$ and F for BF_4^-) will be annotated as Hn−X, where n represents the hydrogen atom under consideration and X denotes the halide atom of the anion. Thus, H2−Cl is used to characterize the Cl atoms of $AlCl_4^-$ coordinated at the cationic H2 atoms.

In Figure 8, we present the cation−anion RDFs for the distances between the geometric center of the imidazolium ring and the central atom of the anion. Table 2 summarizes the peak positions and integrals for the first peak in these RDFs. Apparently, the choice of the anion affects the shape of the RDFs only slightly. However, the density effect produces shorter distances for the BF_4^--based ILs in comparison with the distances for those containing $AlCl_4^-$. Also, the alkyl chain effect is less represented in these RDFs with the exception of a short distance shoulder in $C_2C_1imAlCl_4$ collapsing into the rest of the peak in $C_4C_1imAlCl_4$. Moreover, the RDFs for BF_4^--based ILs produce straighter peaks than do the $AlCl_4^-$-containing ILs. The ranked RDFs, also included in Figure 8, do not provide much information about the structural difference between the first coordinated anions.

In Figure 9, we depicted the RDFs for the Hn−X distances. The positions of the first peak maxima and integrals are summarized in Table 3. The most probable distance (first peak position) between the considered atoms is in very good agreement with previously published QM calculations[62] and

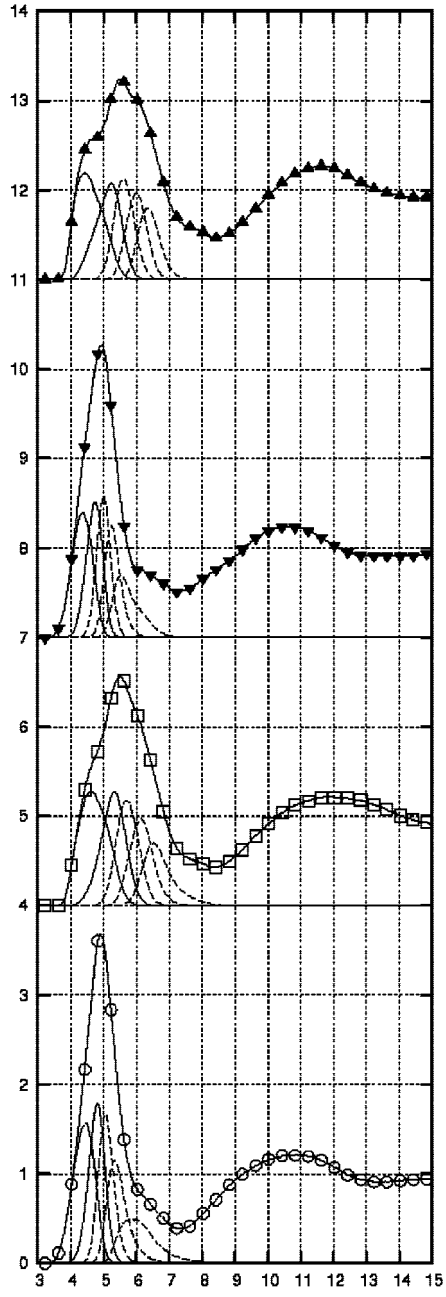

Figure 8. Cation−anion RDFs for the studied ILs from Table 1: ▲ (and shifted by 11), $C_2C_1imAlCl_4$; ▼ (and shifted by 7), $C_2C_1imBF_4$; □ (and shifted by 4), $C_4C_1imAlCl_4$; and ○, $C_4C_1imBF_4$. For each IL, the partial RDFs for the first five neighbors (the low-intensity functions, from left to right in going from the first to the fifth nearest neighbor) are also presented.

TABLE 2: Positions (in Angstroms) and Integrals for the First Peak in the Cation−Anion RDFs

IL	position	integral
$C_2C_1imAlCl_4$	8.375	7.52
$C_4C_1imAlCl_4$	8.425	6.34
$C_2C_1imBF_4$	7.225	6.58
$C_4C_1imBF_4$	7.375	5.72

other simulation studies.[63] Moreover, the integrals exhibit coordination numbers between 2 and 4, indicating that there is only a single anion surrounding each of the hydrogen atoms. Considering equivalent peak integrals and positions for the RDFs involving H4 and H5 atoms, two coordinating regions for the

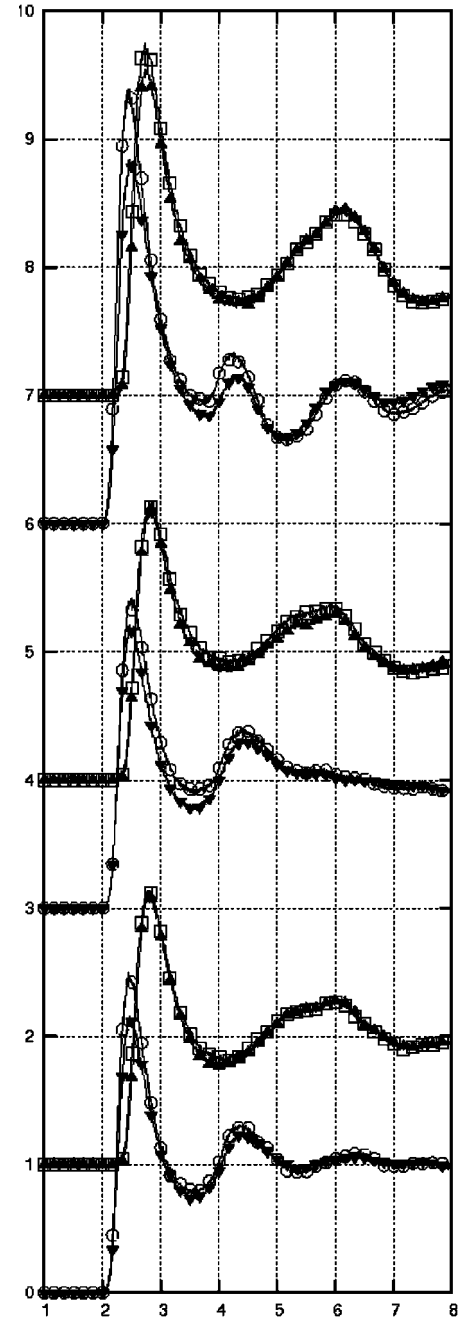

Figure 9. RDFs for correlations of the imidazolium-ring hydrogen atoms and the peripheral atoms X of the anions: ▲, $C_2C_1imAlCl_4$; ▼, $C_2C_1imBF_4$; □, $C_4C_1imAlCl_4$; and ○, $C_4C_1imBF_4$. H2−X RDFs are shifted by 6, and H4-X RDFs are shifted by 3. Nonshifted RDFs correspond to H5−X distances. All of the $AlCl_4^-$-based RDFs were additionally shifted by 1.

TABLE 3: Positions (in Angstroms) and Integrals for the First Peak in the H*n*−X RDFs

	H2-X		H4-X		H5-X	
IL	pos	int	pos	int	pos	int
$C_2C_1imAlCl_4$	2.73	3.71	2.86	3.38	2.76	3.49
$C_4C_1imAlCl_4$	2.74	3.56	2.84	3.14	2.84	2.78
$C_2C_1imBF_4$	2.46	4.21	2.46	2.70	2.46	2.64
$C_4C_1imBF_4$	2.47	3.74	2.50	2.67	2.44	2.26

anions around the cations are distinguished: around the H2 atom (front) and at both the H4 and H5 atoms (behind).

In Figure 10, we present the cation−anion SDFs representing the distribution sampled around the *y* axis and projected into

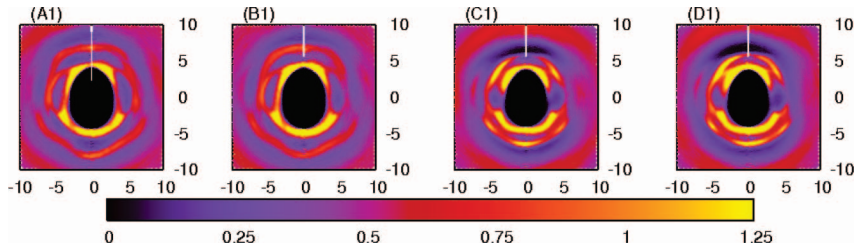

Figure 10. Cation−anion SDFs measured around the *y* axis and projected into the *xy* plane: (A1) $C_2C_1imAlCl_4$, (B1) $C_4C_1imAlCl_4$, (C1) $C_2C_1imBF_4$, and (D1) $C_4C_1imBF_4$.

the *xy* plane. In general, one notices similar trends in the anion distributions. First, the anions surround the H2, H4, and H5 sites. This is expected because these hydrogens are not buried by other atoms, concentrate most of the cation's net charge, and possibly bond to the anions by hydrogen bonds. Also, this is in perfect agreement with the RDFs from Figure 9. Moreover, the anions bonded to H4 and H5 are shared because of their close proximity without bulky groups between them. However, H2 bonds to a single anion. These anions are probably bonded to another cation (Figure 4 permits this conclusion), possibly forming a polymer-like chain. Moreover, a reduced anion distribution around the increasing alkyl chain (from ethyl to *n*-butyl) becomes apparent in Figure 10, as a consequence of steric effects.

In the accompanying Supporting Information, we have included in Figure S3 the anion distribution around the cation's *x* axis projected into the *xz* plane, as well as in Figure S4 the sampling of the anions distributed around the *z* axis and projected into the *yz* plane. Both Figures represent contour plots with warmer colors indicating larger probabilities. Figure S4 also contains the SDFs for the first and second nearest neighbors. Compared with Figure 10, Figures S3 and S4 exhibit different trends. In the BF_4^--based ILs, no significant probabilities for finding the anion above and below the imidazolium ring have been detected. On the other side, strong contributions in these regions are present in the $AlCl_4^-$ ILs. These Figures indicate a preferred above and below coordination of $AlCl_4^-$ but favor front and behind coordination for BF_4^-.

Combining these observations with the conclusions for the anion effects on the cation stacking from the previous section, we suggest that larger anions (and less dense ILs) imply not only a reduction of the range of stacking but also a preferred placement of anions above and below the cation's imidazolium-ring plane. These anions are not only strictly coordinated to the ring but also allow that other cations coordinate preferentially through front or behind sites, introducing a perpendicular configuration between the cations that contrasts with the stacking trend in ILs. On average, our data indicate that each stacked cation pair possesses one anion above and another one below and that each of these anions forms a pair with front or behind coordinating cations, perpendicular to the stacked pair in the $AlCl_4^-$-based ILs.

However, the BF_4^- (smaller anion, more dense IL)-based ILs contain anions concentrated basically at the front and behind coordinating sites. Combining this observation with the stacking behavior of cations, one might expect a larger range of stacking with the anions piled up in the front and behind positions of the cations, at least considering the average liquid-phase configurations of these ILs.

The cation−anion 3D SDFs, included in Figure 6, reflect the cation−anion ionic liquid structure to be in good agreement with the experimental expectations.[54,55] However, the computed 3D SDFs predict a lack of anion probability density in front of the imidazolium protons at a C−H *n*−X angle of 0°. The first contact pairs in the simulations are found with angles between 10 and 35°. This is a commonly known artifact in MD simulations on ILs by force fields based on point charges for the representation of electrostatic interactions, as already discussed in the literature.[22] Moreover, the literature also points out that quantum molecular dynamics calculations[27] as well as more complex force fields including polarization effects in the intermolecular interaction potentials[31] can overcome this limitation.

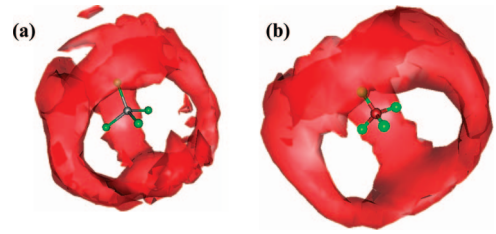

Figure 11. Three-dimensional SDFs at the isosurface of 2.25 for the (a) $AlCl_4^-$ and (b) BF_4^- anions surrounded by imidazolium rings of $C_2C_1im^+$.

In Figure 11, we present the 3D SDFs of the cations surrounding the BF_4^- and $AlCl_4^-$ anions. We emphasize that there are only small differences in these functions for the $C_2C_1im^+$ and $C_4C_1im^+$ cations. Thus, results are illustrated only for the $C_2C_1im^+$-based ILs. From Figure 11, it becomes evident that the anion tends to bind as many of the electron donor atoms as possible, producing a density distributions of cations over the faces of the anion's tetrahedra. This is, as mentioned above, in contrast to what is reported in the literature from QM calculations,[27,29] in which the preferential coordination of a cation to only one halide atom of the anion is revealed. The difference observed here is probably due to density effects in the condensed phase that are not present in the QM calculations on gas-phase structures.

3.3. Anion−Anion Structure. In this section, we present details on the anion−anion structure in the studied ILs. It has been revealed before[37] that the choice of simple spherical anions does not affect the relative structure of the anions in the ILs but interferes with the cation−cation arrangements sustaining or breaking the structural features exposed in section 3.1. Figure 12 presents the calculated RDFs for the pairs of anions in the studied ILs in terms of the peripheral (halide) atoms as well as the central atoms. Comparing the BF_4^- anions with the $AlCl_4^-$ anions, we find that the peak positions of the first maxima are shifted by approximately 1 Å toward larger distances in the ILs containing the larger $AlCl_4^-$ anions. However, the $AlCl_4^-$-based ILs exhibit a prepeak to the first maxima. The appearance of this short-range configuration corroborates our proposal that some $AlCl_4^-$ anions coordinate above and below the imidazolium rings whereas BF_4^- anions do not.

Also, it becomes evident that the ILs composed of $C_4C_1im^+$ cations present larger positions for the first maxima than do

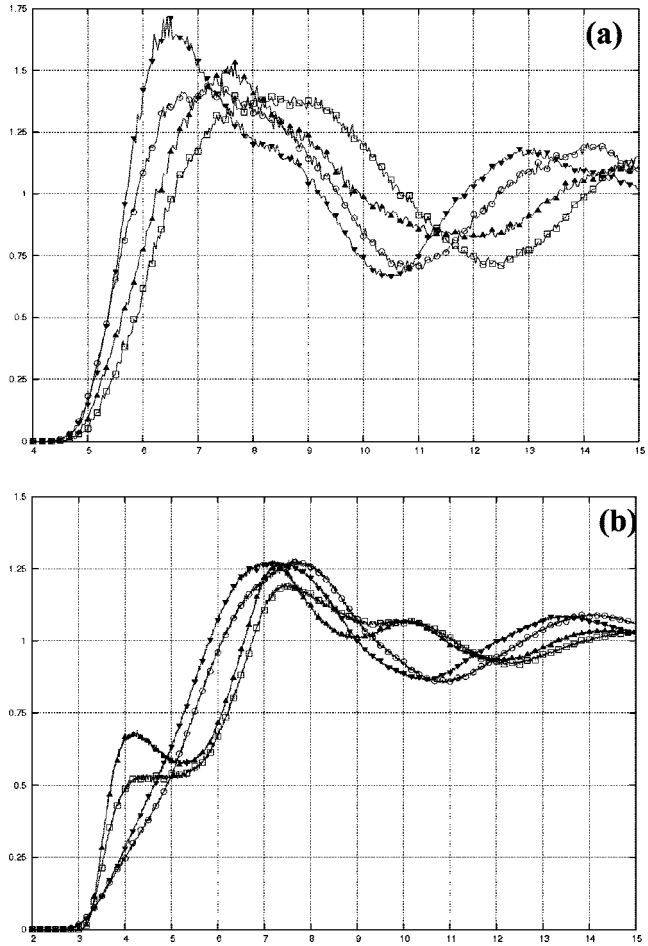

Figure 12. (a) Central and (b) peripheral atom anion RDFs of the studied ILs: ▲, $C_2C_1imAlCl_4$; ▼, $C_2C_1imBF_4$; □, $C_4C_1imAlCl_4$; and ○, $C_4C_1imBF_4$.

TABLE 4: Intermolecular Energies *U* and their Breakdown into Electrostatic U_{el} and Short-Range Contributions U_{vdw}[a]

IL	U	U_{el}	U_{vdw}
$C_2C_1imAlCl_4$	-485.7 ± 8.4	-399.0 ± 8.5	-86.7 ± 0.4
$C_4C_1imAlCl_4$	-467.4 ± 12.1	-375.4 ± 10.4	-92.0 ± 3.7
$C_2C_1imBF_4$	-494.8 ± 5.3	-441.5 ± 0.3	-53.3 ± 5.3
$C_4C_1imBF_4$	-499.3 ± 4.1	-435.5 ± 4.0	-63.7 ± 0.4

[a] Units are kJ/mol.

the $C_2C_1im^+$-based ILs. Thus, shorter alkyl groups (here, ethyl compared with butyl) produce a slightly tighter packing of anions, probably as a consequence of density effects.

3.4. Internal Energies. In this section, we present a discussion of the interaction energies of the studied ILs. In Table 4, we resume the intermolecular potential energy contributions originating in electrostatic and van der Waals interactions from the MD simulations of the four ILs. As expected for these ionic systems, the electrostatic contributions strongly surpass the van der Waals interaction. In addition, it becomes evident that the $AlCl_4^-$-based ILs produce stronger van der Waals interactions, as one might expect from the comparison of the Lennard-Jones parameters for the fluorine and chlorine atoms. The BF_4^--containing ILs are more strongly bound electrostatically because of the increased tendency of imidazolium-ring packing around the smaller anion. The data in Table 4 also demonstrate that the larger alkyl group in the $C_4C_1im^+$-based ILs reduces the electrostatic attraction and increases the van der Waals contribution. The alkyl substituents essentially represent centers for van der Waals interactions possessing weak positive charges on the hydrogen atoms. Thus, considering stacked cation configurations, the alkyl−alkyl interactions favor van der Waals attractions and electrostatic repulsions.

4. Conclusions

This article describes common and advanced structural analysis from MD simulations on several ILs. Four ionic liquids, $C_2C_1imAlCl_4$, $C_2C_1imBF_4$, $C_4C_1imAlCl_4$, and $C_4C_1imBF_4$, were investigated by the use of previously published AMBER-type classical force fields. The results support the cation stacking behavior and range as revealed from experimental measurements. The dependence of the range of stacking on anion choice is due to size and density effects. Differences in stacking are explained in terms of cation−anion coordination above and below the imidazolium-ring planes. This kind of anion coordination breaks the cation−cation sequence in the stacking and causes a perpendicular cation−cation sequence. We suggest the stacking of, on average, two cations in ILs with large anions being increased for the smaller anions. Also, the coordination of the anions to imidazolium-ring hydrogens reveals features of hydrogen bonding, as expected from experiment. An anion-size-dependent proposal for the ILs structure is suggested.

Moreover, it is shown that smaller anions lead to stronger electrostatic contributions to the intermolecular energy, whereas longer alkyl chains result in larger van der Waals contributions. In addition, both larger alkyl chains and smaller anions predict smaller self-diffusion coefficients. We conclude that the use of classical force fields in simulations on ionic liquids permits the elucidation of many properties of ILs, especially their structural details and their relation to other physical properties.

Acknowledgment. This work was supported by the Brazilian agency CNPq (processes 301837/2006-6 and 476661/2006-4). E.S. Böes and J. de Andrade acknowledge scholarships from Brazilian agencies CAPES and CNPq, respectively.

Supporting Information Available: Cation OCFs containing correlations between molecular *x* axes and molecular *y* axes. Cation−anion SDFs measured around the *x* axis and projected into the *xz* plane and measured around the *z* axis and projected into the *yz* plane. This material is available free of charge via the Internet at http://pubs.acs.org.

References and Notes

(1) Horvath, I. T.; Anastas, P. T. *Chem. Rev.* **2007**, *107*, 2169.
(2) Jessop, P.; Leitner, W. *Chemical Synthesis Using Supercritical Fluids*; Wiley-VCH: Weinheim, Germany, 2007.
(3) Horvath, I. T. *Acc. Chem. Res.* **1998**, *31*, 641.
(4) *Ionic Liquids IIIA/B: Fundamentals, Progress, Challenges, and Opportunities*; Rogers, R. D., Seddon, K. R. Eds.; ACS Symposium Series 901/902; American Chemical Society: Washington, DC, 2005.
(5) (a) For vapor pressure measurements of ILs, see Zaitsau, D. H.; Kabo, G. J.; Strechan, A. A.; Paulechka, Y. U.; Tschersich, A.; Verevkin, S. P.; Heintz, A. *J. Phys. Chem. A* **2006**, *110*, 7303. (b) Emel'yanenko, V. N.; Verevkin, S. P.; Heintz, A. *J. Am. Chem. Soc.* **2007**, *129*, 3930.
(6) *Ionic Liquids in Synthesis*; Wasserscheid, P., Welton, T. Eds.; Wiley-VCH: Weinheim, Germany, 2003.
(7) (a) Wishart, J. F.; Castner, E. W., Jr. *J. Phys. Chem. B* **2007**, *111*, 4639. and other articles from the special edition on *The Physical Chemistry of Ionic Liquids.* (b) J. Phys. Chem. B 2007, *111* (18).
(8) Dymek, C. J., Jr.; Stewart, J. J. P. *Inorg. Chem.* **1989**, *28*, 1472.
(9) Takahashi, S.; Curtiss, L. A.; Gosztola, D.; Koura, N.; Saboungi, M. *Inorg. Chem.* **1995**, *34*, 2990.
(10) Carper, W. R.; Mains, G. J.; Piersma, B. J.; Mansfield, S. W.; Larive, C. K. *J. Phys. Chem.* **1996**, *100*, 4724.
(11) Takahashi, S.; Suzuya, K.; Kohara, S.; Koura, N.; Curtiss, L. A.; Saboungi, M. *Z. Phys. Chem.* **1999**, *209*, 209.

(12) Mains, G. J.; Nantsis, E. A.; Carper, W. R. *J. Phys. Chem. A* **2001**, *105*, 4371.
(13) Meng, Z.; Dölle, A.; Carper, W. R. *THEOCHEM* **2002**, *585*, 119.
(14) Turner, E. A.; Pye, C. C.; Singer, R. D. *J. Phys. Chem. A* **2003**, *107*, 2277.
(15) Talaty, E. R.; Raja, S.; Storhaug, V. J.; Dölle, A.; Carper, W. R. *J. Phys. Chem. B* **2004**, *108*, 13177.
(16) Wang, Y.; Li, H.; Han, S. *J. Chem. Phys.* **2005**, *123*, 174501.
(17) Wang, Y.; Li, H.; Han, S. *J. Chem. Phys.* **2006**, *124*, 044504.
(18) Hunt, P. A.; Gould, I. R. *J. Phys. Chem. A* **2006**, *110*, 2269.
(19) Dhumal, N. R. *Chem. Phys.* **2007**, *342*, 245.
(20) Hunt, P. A.; Gould, I. R.; Kirchner, B. *Aust. J. Chem.* **2007**, *60*, 9.
(21) For ionic liquids, see Berg, R. W. *Monatsh. Chem. Chem. Mon.* **2007**, *138*, 1045.
(22) For a summary of the classical simulation methodologies applied to imidazolium-based ILs, see Hunt, P. A. *Mol. Simul.* **2006**, *32*, 1.
(23) Wang, Y. T.; Izvekov, S.; Yan, T. Y.; Voth, G. A. *J. Phys. Chem. B* **2006**, *110*, 3564.
(24) Wang, Y.; Voth, G. A. *J. Phys. Chem. B* **2006**, *110*, 18601.
(25) Bhargava, B. L.; Devane, R.; Klein, M. L.; Balasubramanian, S. *Soft Matter* **2007**, *3*, 1395.
(26) Del Pópolo, M. G.; Lynden-Bell, R. M.; Kohanoff, J. *J. Phys. Chem. B* **2005**, *109*, 5895.
(27) Bühl, M.; Chaumont, A.; Schurhammer, R.; Wipff, G. *J. Phys. Chem. B* **2005**, *109*, 18591.
(28) Bhargava, B. L.; Balasubramanian, S. *Chem. Phys. Lett.* **2005**, *417*, 486.
(29) Bhargava, B. L.; Balasubramanian, S. *J. Phys. Chem. B* **2007**, *111*, 4477.
(30) Bagno, A.; D'Amico, F.; Saielli, G. *Chem. Phys. Chem.* **2007**, *8*, 2007.
(31) Yan, T. Y.; Burnham, C. J.; Del Poolo, M. G.; Voth, G. A. *J. Phys. Chem. B* **2004**, *108*, 11877.
(32) Youngs, T. G. A.; Hardacre, C. *J. Phys. Chem.* **2008**, submitted.
(33) de Andrade, J.; Böes, E. S.; Stassen, H. *J. Phys. Chem. B* **2002**, *106*, 3546.
(34) de Andrade, J.; Böes, E. S.; Stassen, H. *J. Phys. Chem. B* **2002**, *106*, 13344.
(35) Cornell, W. D.; Cieplak, P.; Bayly, C. I.; Gould, I. R.; Merz, K. M.; Ferguson, D. M.; Spellmeyer, D. C.; Fox, T.; Caldwell, J. W.; Kollman, P. A. *J. Am. Chem. Soc.* **1995**, *117*, 5179.
(36) de Andrade, J.; Böes, E. S.; Stassen, H. In *Ionic Liquids IIIA/B: Fundamentals, Progress, Challenges, and Opportunities*; ed. Rogers, R. D., Seddon, K. R. Eds.; ACS Symposium Series 901/902; American Chemical Society: Washington, DC, 2005; p 118.
(37) Dupont, J. *J. Braz. Chem. Soc.* **2004**, *15*, 341.
(38) Canongia Lopes, J. N. A.; Pádua, A. A. H. *J. Phys. Chem. B* **2006**, *110*, 3330.
(39) Dibrov, S. M.; Kochi, J. K. *Acta Crystallogr. C* **2006**, *62*, o19.
(40) Kölle, P.; Dronskowski, R. *Inorg. Chem.* **2004**, *43*, 2803.
(41) Consorti, C. S.; Suarez, P. A. Z.; de Souza, R. F.; Burrow, R. A.; Farrar, D. H.; Lough, A. J.; Loh, W.; da Silva, L. H. M.; Dupont, J. *J. Phys. Chem. B* **2005**, *109*, 4341.
(42) Elaiwi, A.; Hitchcock, P. B.; Seddon, K. R.; Srinivasan, N.; Tan, Y.; Welton, T.; Zora, J. A. *J. Chem. Soc., Dalton Trans.* **1995**, 3467.
(43) Wilkes, J. S.; Zaworotko, M. J. *J. Chem. Soc., Chem. Commun.* **1992**, 965.
(44) Suarez, P. A.; Einloft, S.; Dullius, J. L.; de Souza, R. F.; Dupont, J. *J. Chim. Phys. Phys.-Chim. Bio.* **1998**, *95*, 1626.
(45) Chiappe, C.; Pieraccini, D. *J. Phys. Org. Chem.* **2005**, *18*, 275.
(46) Wang, Y.; Voth, G. A. *J. Am. Chem. Soc.* **2005**, *127*, 12192.
(47) Lyubartsev, A. P.; Laaksonen, A. *Comput. Phys. Commun.* **2000**, *128*, 565.
(48) Nosé, S. *Mol. Phys.* **1984**, *52*, 525.
(49) Tuckerman, M.; Berne, B. J. *J. Chem. Phys.* **1992**, *97*, 1990.
(50) Ewald, P. *Ann. Phys.* **1921**, *64*, 253.
(51) Gray, C. G.; Gubbins, K. E. *Theory of Molecular Fluids: Fundamentals*, Clarendon Press: Oxford, 1984;*Vol 1*.
(52) Avent, A. G.; Chaloner, P. A.; Day, M. P.; Seddon, K. R.; Welton, T. *J. Chem. Soc., Dalton Trans.* **1994**, 3405.
(53) Bonhote, P.; Dias, A. P.; Papageorgiou, N.; Kalyanasundaram, K.; Grätzel, M. *Inorg. Chem.* **1996**, *35*, 1168.
(54) Hardacre, C.; Holbrey, J. D.; McMath, S. E. J.; Bowron, D. T.; Soper, A. K. *J. Chem. Phys.* **2003**, *118*, 273.
(55) Hardacre, C.; McMath, S. E. J.; Nieuwnhuyzen, M.; Bowrin, D. T.; Soper, A. K. *J. Phys.: Condens. Matter* **2003**, *15*, S159.
(56) Fannin, A. A., Jr.; Floreani, D. A.; King, L. A.; Landers, J. S.; Piersma, B. J.; Stech, D. J.; Vaughn, R. L.; Wilkes, J. S.; Williams, J. L. *J. Phys. Chem.* **1984**, *88*, 2614.
(57) Fuller, J.; Carlin, R. T.; Osteryoung, R. A. *J. Eletrochem. Soc.* **1997**, *144*, 3881.
(58) Hagiwara, R.; Ito, Y. *J. Fluorine Chem.* **2000**, *105*, 221.
(59) Lopes, J.; Pádua, A. *J. Phys. Chem. B* **2004**, *108*, 16893.
(60) Lee, S. U.; Jung, J.; Han, Y. *Chem. Phys. Lett.* **2005**, *406*, 332.
(61) Salanne, M.; Simon, C.; Turq, P. *J. Phys. Chem. B* **2006**, *110*, 3504.
(62) Liu, Z.; Huang, S.; Wang, W. *J. Phys. Chem. B* **2004**, *108*, 12978.
(63) Schröder, G.; Rudas, T.; Steinhauser, O. *J. Chem. Phys.* **2006**, *125*, 244506.

JP801445J